Do river profiles record along-stream variations of low uplift rate?

S. Carretier,[1] B. Nivière,[2] M. Giamboni,[3,4] and T. Winter[5]

Received 5 October 2005; revised 21 February 2006; accepted 1 March 2006; published 28 June 2006.

[1] Spatial variations of gradients in landscapes may be used to identify and quantify recent deformation. The problem with doing this is to determine whether tectonic or climatic forcing is responsible for these variations, especially for low uplift rate environments ($\ll$1 mm yr^{-1}) where climate changes may have erased tectonic features. We evaluate the respective contribution of low uplift rate ($\sim$0.1 mm yr^{-1}) and Pleistocene climate oscillations on gradient variations of two comparable river profiles crossing different uplift zones in the southern Upper Rhine Graben. We compare the observed points of discontinuity in river profile (knickpoints) and convex portions (knickzones) with those predicted by a detachment-limited model that includes stochastic short-term and cyclic long-term variations in climate, a bedrock detachment threshold and rock uplift. The detachment-limited model is chosen as it predicts the development of persistent knickpoints. Differing values of the shear stress exponent, erosion threshold, climate variability and uplift pattern have been checked. Our modeling suggests that climate changes had no significant effects on profiles and that anomalies are more likely due to anticline growth. This surprising result arises from the combination of a very low regional uplift rate and the detachment-limited assumption. The detachment-limited model implies an upstream propagation of knickpoints and knickzones generated by uplift at the outlet during dry climate periods of low erosion. The greater the uplift rate, the larger the variations in river bed elevation. Thus, for high uplift rate, knickpoints and knickzones generated by climate oscillations are more likely to hide tectonic features. This result seems counterintuitive because it suggests that tectonic knickzones will be better preserved in low uplift rate environments, provided that the lithology is homogeneous.

Citation: Carretier, S., B. Nivière, M. Giamboni, and T. Winter (2006), Do river profiles record along-stream variations of low uplift rate?, *J. Geophys. Res.*, *111*, F02024, doi:10.1029/2005JF000419.

1. Introduction

[2] In this paper, we evaluate whether rock uplift or climate variations are responsible for knickpoints observed in the profiles of two rivers, the Largue and Ill Rivers, located in a low uplift rate ($\sim$0.1 mm yr^{-1}) region, the Sundgau area in the Upper Rhine Graben (France). The question of the origin of geomorphic features is fundamental in the field of active tectonics because topographic features may be used to infer cumulative displacements on faults and folds [e.g., *Molnar et al.*, 1994; *Lavé and Avouac*, 2000; *Carretier et al.*, 2002]. The answer is usually difficult because geomorphic features result from various tectonic- erosion interactions which may lead to similar forms. One may suppose that in low uplift rate settings and semiarid to humid climates, erosion will hamper the geomorphic response to tectonics. For example, if we assume an uplift rate of 0.1 mm yr^{-1}, 1 m uplift will require 10 ky, a time span during which erosion and deposition may destroy such a small tectonic relief. Furthermore, assessing strain rates and seismic hazard in areas of low tectonic activity requires geomorphological markers that can record several seismic cycles. Because the mean recurrence time of events on slow structures may reach several thousand years to more than 10 ky [e.g., *Camelbeeck and Meghraoui*, 1998], the geomorphic record of uplift on such structures requires the preservation of markers on time spans of several 100 ky. Over such durations, climate variations may erase tectonic markers and produce ambiguous features such as knickpoints and rapid incision in rivers [*Whipple*, 2001; *Zaprowski et al.*, 2005].

[3] Tectonic geomorphology methods have been used in numerous studies to analyze active structures (see Table 1). Dating deformed markers is the most efficient method, but deformed markers are not easy to identify in slowly uplifting humid areas. Morphometry based on conceptual or analogue models provides useful insight but lacks a theoretical basis permitting the quantification of uplift rates. Finally, morphometry based on mechanistic modeling of erosion has

[1]Institut de Recherche pour le Développement, Laboratoire des Mécanismes de transfert en Géologie, UMR5563, Université Paul Sabatier, Toulouse, France.
[2]Université de Pau et des pays de l'Adour, UMR5112, Pau, France.
[3]Protective Forests and Natural Hazards, Swiss Forest Agency, Bern, Switzerland.
[4]Also at University of Basel, Basel, Switzerland.
[5]Bureau de Recherches Géologiques et Minières, Hazard Mechanisms and Simulation Unit, Orleans, France.

0148-0227/06/2005JF000419

Table 1. Geomorphological Methods Used to Analyze Active Structures

Description	References
Dating of deformed linear or planar markers (alluvial fans, fluvial terraces)	[e.g., *Ritz et al.*, 2003; *Rockwell et al.*, 1984; *Molnar et al.*, 1994; *Siame et al.*, 1997]
Variations of erosion or incision rates	[e.g., *Pazzaglia and Brandon*, 2001; *Lavé and Avouac*, 2000; *Wobus et al.*, 2005; *Krzyszkowski et al.*, 2000; *Maddy et al.*, 2000]
Morphometry based on conceptual models or experiments on fluvial systems disrupted by tectonics	stream gradient index [e.g., *Hack*, 1973; *Seeber and Gornitz*, 1983]
	local relief [e.g., *Hurtrez et al.*, 1999]
	stream channel deflections [e.g., *McGill and Sieh*, 1991; *Gaudemer et al.*, 1989; *Jackson et al.*, 1996]
	change in river sinuosity [e.g., *Ouchi*, 1985; *Giamboni et al.*, 2005]
	valley asymmetry [e.g., *Cox*, 1994]
	terrace long profile geometry [e.g., *Merritts et al.*, 1994]
Morphometry based on a mechanical modeling of erosion	marine and fluvial terrace morphology [e.g., *Rosenbloom and Anderson*, 1994; *Arrowsmith et al.*, 1996]
	river incision and width [e.g., *Lavé and Avouac*, 2001]
	ratio of alluvial fan and drainage basins areas [e.g., *Whipple and Trayler*, 1996; *Allen and Densmore*, 2000]
	steepness index [e.g., *Lague et al.*, 2000; *Kirby and Whipple*, 2001; *Hodges et al.*, 2004]
	river deviation [e.g., *Tomkin and Braun*, 1999]

provided significant constrains on tectonic and erosion rates at the fault scarp scale [e.g., *Hanks*, 1999] but at the scale of drainage basin, this approach has suffered from uncertainties in erosion laws [e.g., *van der Beek and Bishop*, 2003; *Tomkin et al.*, 2003]. Moreover, many studies at this scale assume a steady state topography that is difficult to demonstrate and may not be the case in many instances [*Whipple*, 2001]. Therefore quantitative methods capable of linking nonequilibrium morphologies and changes in tectonic uplift or climate are badly needed.

[4] This paper is an attempt to give a physically based interpretation to knickpoints and knickzones observed in two rivers in a low uplift rate area. We define a knickpoint as a point of discontinuity in a river profile, that corresponds to either an abrupt change in slope or in bed elevation. We use the term knickzone to describe a portion of a profile which is broadly convex over several kilometers above knickpoints [e.g., *Zaprowski et al.*, 2001]. We focus on river profiles because rivers transmit tectonic uplift to drainage basin slopes with a time delay. Thus current river profile anomalies may be caused by uplift rate variations which occurred several tens of thousand of years ago [e.g., *Whipple and Tucker*, 1999]. This is the relevant time span to analyze slow deformation, which makes river profiles good candidates to record past and current deformation. In order to evaluate whether the knickpoints have a climatic or tectonic origin, we analyze the fit between observed profiles and synthetic ones obtained with a fluvial incision model subjected to climate oscillations (100 ky) and along-profile uplift rate variations. The river evolution model was proposed by *Tucker and Bras* [2000] and *Tucker* [2004] to model detachment-limited incision, including stochastic rainfall variability and a detachment threshold.

[5] In the following we present the tectonic environment and the rivers, justify the choice of the model and describe the fitting procedure. The fit for various model parameters and climatic scenarios is analyzed and we discuss some possible generalization of our results.

2. Tectonic and Geomorphological Settings

[6] The 50 × 50 km Sundgau region is located between the more external northern emergent front of the Mio-Pliocene Western Alps (the Jura fold and thrust belt) and the southern end of the late Eocene Upper Rhine Graben (URG) (Figure 1a). The geological evolution of this area is well known and has been synthesized by, for example, *Sissingh* [1998], *Schumacher* [2002] and *Dèzes et al.* [2004] for the URG and by [*Laubscher*, 2001] for the Jura Mountains. We focus here on the relation of the Sundgau drainage network with the Plio-Pleistocene folding of the area based on the works of *Nivière and Winter* [2000] and *Giamboni et al.* [2004a, 2004b, 2005].

[7] The area is located above a WSW-ENE Variscan transform zone that was potentially reactivated during the late Eocene rifting of Western Europe [*Schumacher*, 2002]. The Oligocene structural inheritance mainly consists of half-grabens controlled by roughly N10E- to N30E-trending west-dipping normal faults, like the Illfurth fault (Figure 1a).

[8] During Middle Miocene time the Alpine thrust front started to propagate farther northward and influenced the area of the Jura Mountains. At the end of Pliocene time, the Alpine front corresponded to EW folds including the Ferrette fold [*Giamboni et al.*, 2004a]. Continued Alpine compression during the Pleistocene was responsible for propagating the deformation northward. The current frontal thrust is located near Mulhouse, on a N70E-trending branch of the Illfurth fault (Figure 1b) [*Nivière and Winter*, 2000]. Between the Ferrette fold and this thrust, several other ~10 km spaced WSW-ENE blind reverse faults formed, rooted ~1000 m deep in Triassic evaporite marls. These faults are post-Pliocene because they have deformed the Pliocene Sundgau Gravels and the Pleistocene terraces of the Rhine river [*Nivière et al.*, 2006]. The Sundgau Gravels correspond to a paleo-Rhine deposit. This marker is assigned a late Zanclean to early Plaisencian age (4.2 to 2.9 My) by *Fejfar et al.* [1998] whereas *Petit et al.* [1996] proposed an age of 3.4–2.6 My. These dates are based on assemblages of rodents and molluscs. The blind faults are associated with WSW-ENE anticlines revealed by the mapping of the base of the Sundgau Gravels [*Giamboni et al.*, 2004a, 2004b] (Figure 1b). These anticlines are themselves associated with topographic ridges, whose elevations decrease from the south (650 m in the Ferrette fold) to the north (300 m) [*Meyer et al.*, 1994; *Nivière*

and Winter, 2000]. The anticlines add to a regional northwards tilting of the base of the Sundgau Gravels [*Giamboni et al.*, 2004a]. The elevation also decreases regularly (slope ~ 1°) from the ~650-m-high southern crest of the Jura topographic front to ~290 m at Mulhouse in the north, the edge of the uplifted domain. This tilting is interpreted to be associated with the development of a tectonic wedge in front of the Jura Belt [*Meyer et al.*, 1994; *Nivière and Winter*, 2000; *Nivière et al.*, 2006]. The tilting of the Sundgau topography and of the base of the Sundgau Gravels allows an estimate of a mean regional post-Pliocene uplift rate relative to the city of Mulhouse of between 0.06 to 0.11 mm yr^{-1} [*Nivière et al.*, 2006].

[9] *Giamboni et al.* [2004a, 2005] analyzed the geomorphology of several rivers flowing northwards across the uplifted area, in particular the Ill and Largue Rivers which are reexamined in this study. Both rivers flow across the Sundgau from the Ferrette fold in the south and join each other 10 km upstream of Mulhouse (Figure 1b). This study focuses on the long profiles of the rivers to Mulhouse, the northern boundary of the uplifted domain (Figure 1b). These profiles have roughly the same length to Mulhouse (50 km), the same relief from the upper part of the Sundgau Gravels to Mulhouse (300 m) and the same drainage areas at their confluence (circa 350 km^2). The drainage area accumulation with distances along the river courses are also very similar (Figure 2a). Their beds are covered by gravel and they incise into Oxfordian and Tertiary units.

[10] *Giamboni et al.* [2005] analyzed the relationship between the stream-gradient index [*Hack*, 1973] along river profiles, lithological transitions, river junctions and the location of anticlines. High values of the stream-gradient index were found at river junctions and at lithological transitions, but the highest values were found above anticlines. High values of the stream-gradient index correspond to knickpoints and knickzones along river profiles. Knickpoints correspond here to discontinuities of river gradient, and there are no waterfalls associated with knickpoints. Figure 2a shows that some knickpoints along the Ill and Largue Rivers correspond to river junctions with large tributaries (large increase of drainage area). Moreover, Figure 2b shows that some of the lithological transitions are associated with knickpoints. Along profiles, the lithology varies between marls and sandstone, clay and marls, and limestones (Figure 2b). Knickpoints at lithological transitions are likely to propagate upstream because stratigraphic contacts are not vertical. The largest variation in river bed gradient and altitude occurs on the Ill profile above the Altkirch fold (Figures 1b and 2a). Here a knickzone (convex portion of the profile) is visible as a ~15 m offset of the river bed over 5 km (Figure 2a). The knickpoint at the foot of the knickzone does not correlate with any major change in drainage area nor lithological transition. This led *Giamboni et al.* [2005] to the conclusion that this knickzone is a geomorphic response to the uplift of the Altkirch fold. If true, the fact that the knickzone has not migrated upstream above the fold implies that the uplift is still persistent. A reach of the Largue River above the Dannemarie fold has a high stream-gradient index [*Giamboni et al.*, 2005] (Figure 2a). It is probably mainly influenced by the lithological transitions above and at the edge of the Dannemarie fold. However, a local uplift may also steepen the river gradient. Current uplift above the Altkirch and Dannemarie folds is also supported by the narrowing of the valley above them [*Giamboni et al.*, 2004a]. Remnants of fluvial terraces were also mapped by *Giamboni et al.* [2004b] along the Ill and Largue Rivers, but their continuity is not clear, so that it is not clear whether they are more numerous or folded above the anticlines.

[11] The present-day climate of the Sundgau area is humid, with annual mean precipitation over the last 30 years of 500 mm. Considering the low relief of the Sundgau and the proximity of both rivers, the climate can be considered as homogeneous over this area.

[12] On the whole, these data suggest that at least the knickzone above the Altkirch fold has a tectonic origin. Nevertheless, it is striking that such low relief features generated by a low uplift rate (in the order of 0.1 mm yr^{-1}) have survived long-term climate variations during the Pleistocene. One could imagine that incision (and deposition) should have smoothed the knickpoints, or that cyclic incision due to climate variations may have generated knickzones with comparable amplitudes. In order to provide some possible explanations of such an apparent paradox, we explore the responses of a river incision model to climate and uplift variations.

3. Modeling Approach

3.1. Long River Profile Model

[13] Different mechanical models of long-term fluvial incision have been proposed, but there is no clear agreement on the broader applicability of one compared to the others [*Stock and Montgomery*, 1999; *van der Beek and Bishop*, 2003; *Tomkin et al.*, 2003]. Actually, very few studies have checked the consistency of the models with natural examples regarding their ability to correctly predict incision, response time and river profile shape [see *Whipple*, 2004]. In parallel, some studies have proposed guidelines to choose

Figure 1. (a) Structural map of the Upper Rhine Graben (URG) (modified after *Nivière and Winter* [2000]). The URG is bordered by the Vosges Mountains to the west, the Black Forest Mountains to the east, and the Jura mountains to the south. The Oligocene structural inheritance consists of N10E- to N30E-trending normal faults, such as the Illfurth fault [e.g., *Dèzes et al.*, 2004]. To the south, the Mesozoic cover of the Jura is faulted and folded in a roughly EW direction. The folding results from the Mio-Pliocene Alpine compression. The Ferrette fold corresponds to the front of the deformation at the end of the Pliocene. (b) Sundgau region. Several EW faults have affected the Sundgau Gravels (2.6–4.2 My) which correspond to a Pliocene alluvial plain of the Rhine river, when it flowed to the west [e.g., *Petit et al.*, 1996]. Folding of the base of Sundgau Gravels is oriented parallel to the trend of the underlying structures. Topographic ridges are found above these folds. The Sundgau Gravels are also tilted northward as well as the topography which decreases from the Ferrette fold (~650 m) to Mulhouse, the edge of the uplifted domain. The Ill and Largue Rivers flow northward across the uplifted and folded region (modified after *Giamboni et al.* [2004b]). DEM source: SRTM NASA.

an appropriate model from the river long profile [see *Whipple and Tucker*, 1999; *Tucker and Whipple*, 2002; *Carretier and Lucazeau*, 2005; *Brocard and van der Beek*, 2006]. We use such guidelines to justify the selected model. The consistency of model predictions is discussed to justify a posteriori the selected model, but it is necessary to keep in mind that the proposed answers to the question addressed in this paper are strongly related to the assumptions of the

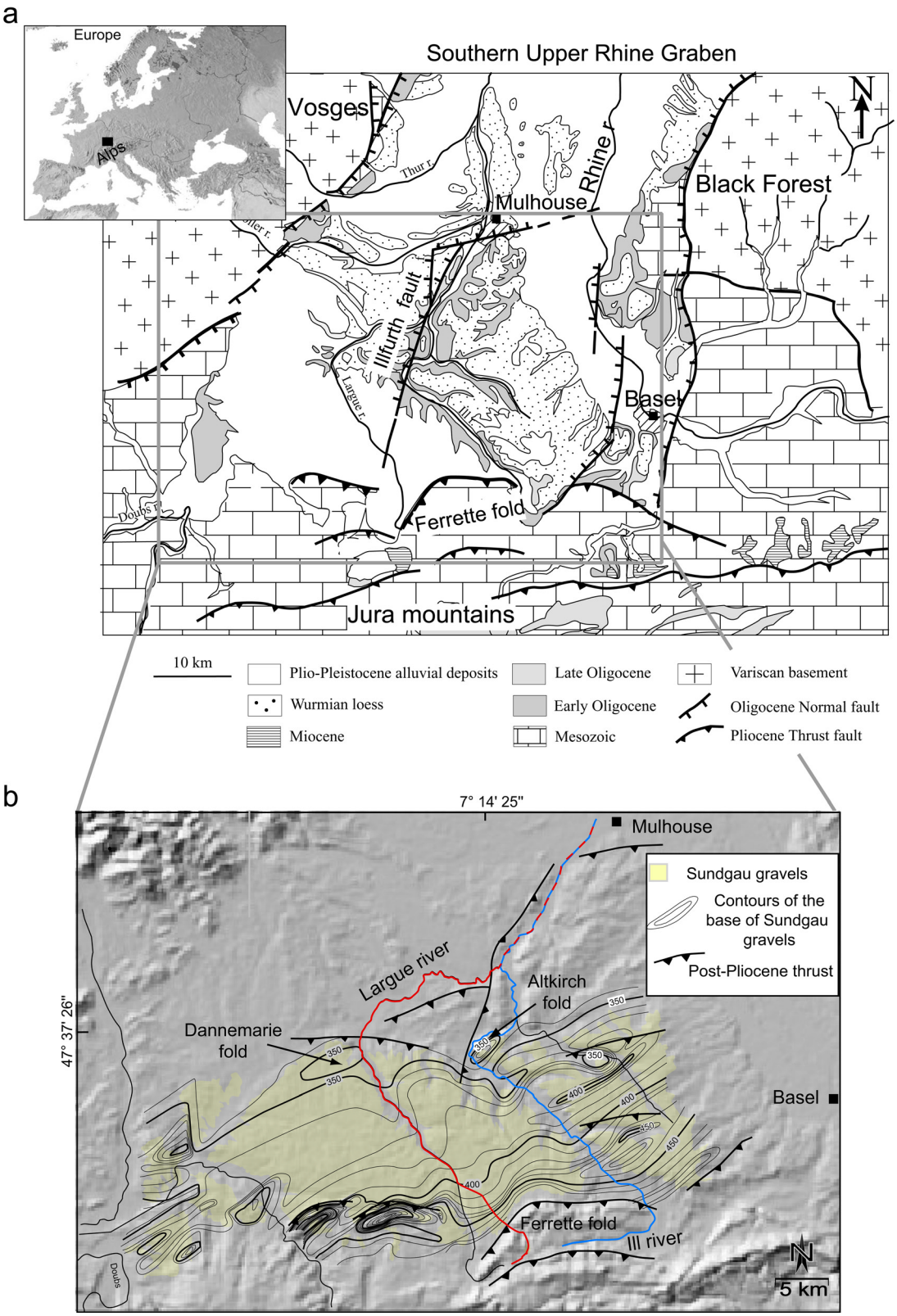

Figure 1

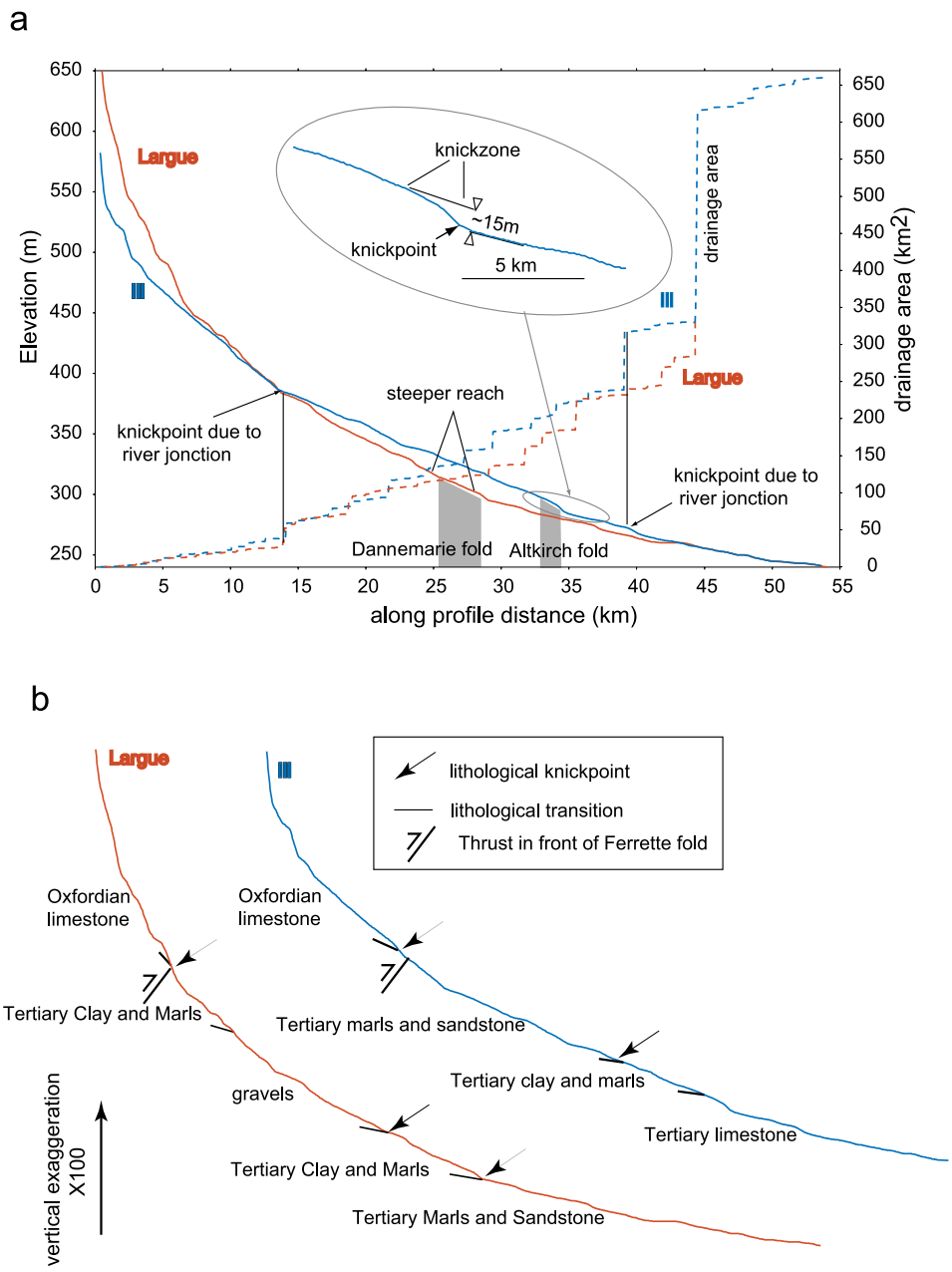

Figure 2. (a) Profiles of the Ill and Largue rivers (see locations on Figure 1b). Profiles have been extracted from 1:25000 scale French topographic maps [*Giamboni et al.*, 2004a]. Drainage area profiles are similar for both rivers ($A = 11.5\ x^{1.6}$). Several knickpoints in the profiles occur at tributary junctions where drainage area increases abruptly. The Pleistocene Dannemarie and Altkirch folds are indicated with gray boxes. A knickzone (convex portion above the point of discontinuity in river slope or knickpoint) appears above the Altkirch fold. This knickzone does not correlate with any major tributary junction nor lithological change. A steep reach appears above the Dannemarie fold, which may be controlled by local uplift and lithological change. Vertical exaggeration is 100X. (b) Lithological changes along the Ill and Largue profiles, with associated knickpoints (after *Giamboni et al.* [2004a]). Vertical exaggeration is 100X.

following model. We use a detachment-limited model, which links the erosion rate to a power law of the excess shear stress applied to the river bed (usually called "shear stress model with threshold") (see Appendix A). This model (with negligible or significant threshold) allows the formation and the long-time preservation of well-marked knickpoints [*Howard et al.*, 1994; *Whipple and Tucker*, 1999] associated with localized uplift or elevation changes at base level. This is not possible with a pure transport-limited model (erosion limited by the ability of the river to transport sediment coming from upstream), which predicts the rapid smoothing of knickpoints [e.g., *Ouchi*, 1985; *Howard et al.*, 1994; *Poisson and Avouac*, 2004]. The sensitivity of gradient to some lithological variations, even

small, is also an argument in favor of detachment-limited behavior, as transport-limited gradients do not depend on the bedrock strength.

[14] Recent studies have explored how erosion models account for the variability of water discharges and their capacity to exceed erosion thresholds [*Tucker and Bras*, 2000; *Crave and Davy*, 2001; *Molnar*, 2001; *Snyder et al.*, 2003a; *Tucker*, 2004; *Lague et al.*, 2005]. The combination of climate variability and erosion thresholds seems to be a necessary condition to predict relevant response times and scaling relationships between uplift and fluvial relief. Thus we use the Stochastic Threshold Model proposed by *Tucker and Bras* [2000] and *Tucker* [2004]. This model combines the shear stress model with a threshold for a storm event with a rectangular Poisson model of discharge distribution. *Tucker* [2004] provided an approximate analytical solution of the long-term mean incision rate of the form (as reformulated by *Snyder et al.* [2003a, 2003b]; see Appendix A),

$$\langle E \rangle = K_R K_C K_{\tau_c} A^m S^n, \tag{1}$$

where K_R encompasses the physical parameters, K_C encompasses the climatic parameters, K_{τ_c} is a threshold term equal to 1 for negligible threshold ($\tau_c = 0$ Pa) and tending asymptotically toward zero for increasing critical runoff (the minimum runoff necessary for particle detachment R_c), A is the drainage area and S the river gradient. The climate is described via two parameters in K_C (see equation (A14)): The variability factor F_{var} is the inverse of the proportion of time with rain [*Tucker and Bras*, 2000], and P is the mean storm rainfall intensity. The mean precipitation rate $\langle P \rangle$ is the ratio of P over F_{var}. For example, an arid climate corresponds to high F_{var} and low $\langle P \rangle$. Although the Poisson model is not a good fit for classical discharge events distribution for small and very large discharge events [*Lague et al.*, 2005], we will see that our main conclusions do not depend critically on the Poisson model.

[15] The long-term height variations of river profiles are modeled using the following equation:

$$\frac{\partial h(x,t)}{\partial t} = -\langle E \rangle + U(x,t), \tag{2}$$

where $h(x, t)$ is the profile elevation function of location along profile x and time t and $U(x, t)$ is an uplift rate function relative to the city of Mulhouse which is located out of the uplifted domain. The time scale over which the mean erosion rate $\langle E \rangle$ converges toward a nearly constant value should be on the order of 10^2–10^3 years (return time of the most rare rainfall events [*Lague et al.*, 2005]). Longer-period variations in $\langle E \rangle$ (e.g., 100 ky) can be obtained by varying the mean and variability of precipitation rates in order to model oscillations between dry and wet periods.

[16] Our approach is a perturbation analysis. It consists of modeling equilibrium profiles with constant parameters, then modeling the impact of climatic changes, and finally modeling the impact of localized uplift. For each scenario, we test the fit between observed and synthetic profiles. These fits help us evaluate the relative contribution of uplift and climate variations on knickzones development. The synthetic profiles are obtained by downstream finite difference integration of equation 2 (~50 years time step, 40 m spatial resolution) with fixed elevation at the outlet. Profiles are modeled from the source to Mulhouse without taking into account lithological variations. Drainage area A along profile is approximated by a power law function of the downstream distance x (Hack's law $A = 11.5\, x^{1.6}$). The fit is evaluated by calculating the standard deviation (STD) between observed and synthetic profiles.

$$\text{STD} = \sqrt{\frac{1}{p-1}\sum_{j=1}^{p}\left(h_{\text{model}}(x_j) - h_{\text{data}}(x_j)\right)^2}, \tag{3}$$

where the j [1, p] refers to the points of the profiles.

3.2. Parameter Values

[17] The values of physical parameters used for the two rivers are discussed in Appendix A. We do not have the value of the variability factor F_{var} in the study area. We fixed F_{var} at 10, which lies within the range of values in the United States [*Tucker*, 2004], but it is not constrained here. In our study, it is fundamental that the model predicts the largest variations of incision rate when the climate varies. If not, the model would not allow us to evaluate the maximum impact of climate change on river profiles and thus to compare the relative impact of climate and uplift. We vary F_{var} in section 4 to evaluate the effects of climate variations. Moreover, adjustment of the unknown parameter k_e (equation (A2)) depends on the choice of F_{var}. In order to evaluate whether our results can critically depend on the choice of these two parameters, we calculate variations in the mean erosion rate $\langle E \rangle$ (equation 1) associated with F_{var} variations. Figure 3a shows these variations for differing values of the critical detachment stress τ_c and the shear stress exponent a (equation (A2)). Each curve corresponds to differing values of k_e, adjusted so that the mean erosion rate equals the uplift rate and the fluvial relief corresponds to that of studied rivers. For the red curves, k_e is adjusted with $F_{\text{var}} = 10$ and for the green curves, with $F_{\text{var}} = 30$. It appears in both cases that 90% variations around these values corresponds to more than 50–70% variation in the mean erosion rate $\langle E \rangle$ (Figure 3a). Thus, even if the value $F_{\text{var}} = 10$ is not correct for the present days or as the mean value over geological time, variation around this value corresponds to the largest fluctuations of mean erosion rate, and thus to the largest possible river profile elevation variations due to climate change. We also plot in Figure 3b the dependence of $\langle E \rangle$ on the mean precipitation rate when it varies around the value $\langle P \rangle = 500$ mm yr^{-1}. This shows that the mean incision rate can increase much more than the tested range, in particular if $a = 5/2$. Nevertheless, we will see that a larger range of values would not change our main conclusion regarding the climatic impact on river profiles.

[18] Three parameters remain undefined: k_e, τ_c and a (Equation (A1)). The exponent a of the shear stress excess can take different values between 1 and 5/2 depending on the main detachment process [*Whipple et al.*, 2000]. As this process can vary over time because of variations of sediment supply (abrasion tool), we test the two extreme values. We point out here that a simplification of the shear stress model with threshold has been used to make an analytical solution tractable (equation (A2)). This leads to a significant

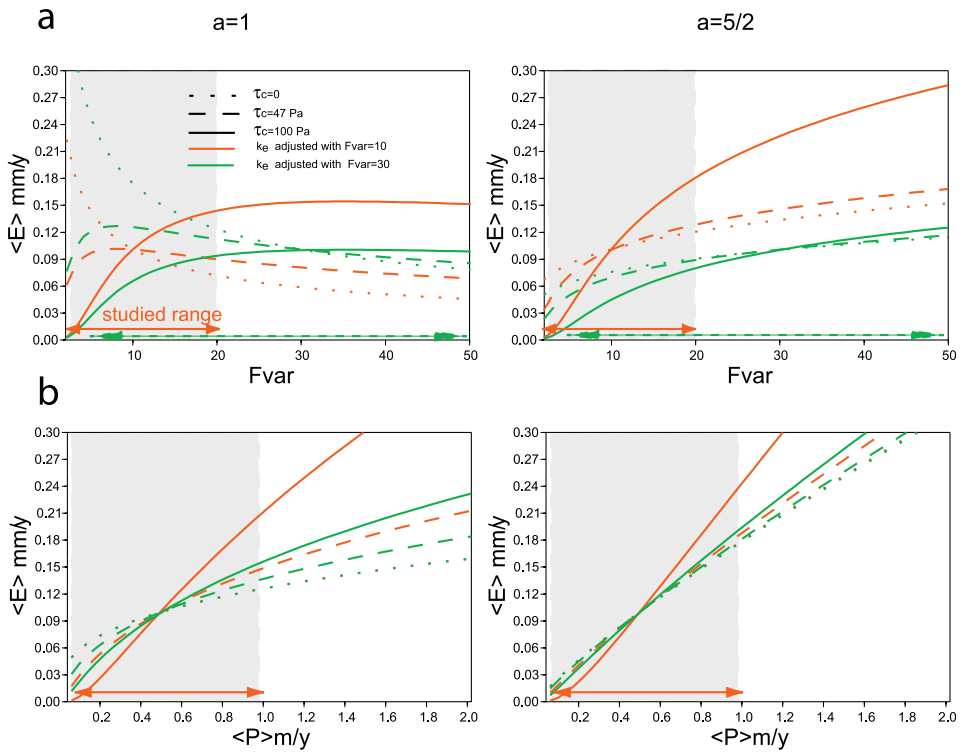

Figure 3. Variations of mean erosion rates $\langle E \rangle$ (equation (1), $S = 0.0025$, $A = 370$ km^2) as function of the variability factor F_{var} and mean precipitation rate $\langle P \rangle$ for differing values of k_e, of the critical shear stress τ_c (0, 47 and 100 Pa) and of the shear stress exponent a (1 and 5/2). Curves correspond to differing values of k_e (the factor linking incision rate and power of excess shear stress in equation (A2)) adjusted to obtain a dynamic equilibrium such that the mean erosion rate $\langle E \rangle$ is 0.1 mm yr^{-1}, the fluvial relief is 212 m (fluvial relief of the Ill and Largue Rivers), all of this for an uplift rate of 0.1 mm yr^{-1} and a precipitation rate $\langle P \rangle = 0.5$ m yr^{-1}. Red curves correspond to adjusted k_e with $F_{var} = 10$ and green curves with $F_{var} = 30$. (a) The horizontal red arrows and the gray domains show the range of variation around $F_{var} = 10$ imposed in experiments where the climate varies. This range corresponds to about 50–70% of the maximum variations of the mean erosion rate. Similar ranges are reached with $F_{var} = 30$ for the same range of variations (green arrows). (b) Mean erosion rate versus mean precipitation rate. This figure suggests that the results of the tested climatic scenarios in terms of incision should not critically depend on the assumed reference value of F_{var}.

overestimation of the erosion rate for the value $a = 5/2$ when the shear stress is close to the critical shear stress. For example, if $\tau = 2 * \tau_c$, the erosion rate predicted by equation (A2) is 4.6 times greater than that predicted by equation (A1). This implies that the modeled incision will be a maximum, which is not a problem if we want to estimate the maximum possible profile variations due to climate change.

[19] It is usually difficult to evaluate the critical shear stress τ_c (equation (A1) [e.g., *Snyder et al.*, 2003a]). Here we assume that the present day river gradients represent gradients below which no detachment occurs ($\epsilon = 0$) for mean discharge conditions. This assumption is partially supported by the presence of gravels covering the bed of the rivers. Using equation (A3) with the mean value Q_m, we estimate a value of τ_c of ~9.5 Pa. In the following, we will use the values of τ_c of 0 Pa, 47 Pa and 100 Pa, in order to evaluate the effect of negligible and significant critical shear stresses on model fits. These values are consistently lower than or equal to other estimates (e.g., ~100–200 Pa for mudstone and sandstone [*Snyder et al.*, 2003a]). In the case where $\tau_c = 0$ Pa, the mean erosion rate (equation (1) simplifies into the classical stream power law ($K_{\tau c} = 1$ in equation 1)). Therefore the comparison of model fits with no or large critical shear stresses will help us discuss the validity of the stream power law and stochastic threshold models in the studied example. The parameter k_e (equation (A2)) remains undetermined. It is adjusted it in the next section.

4. Results

4.1. Initial Equilibrium Profiles

[20] An interesting feature of the Ill and Largue River profiles is their close similarity consistent with the fact that they flow over the same uplifted initial surface. We assume a common initial profile for the two rivers. This profile is determined such that a dynamic equilibrium profile fits the fluvial relief at 6 km from the source. We do not study the fit between 0 and 6 km because the rivers flow across significantly differing lithologies (and potentially uplift rates) in this portion compared to the Tertiary units exposed downstream. Varying τ_c along the profile would allow us to

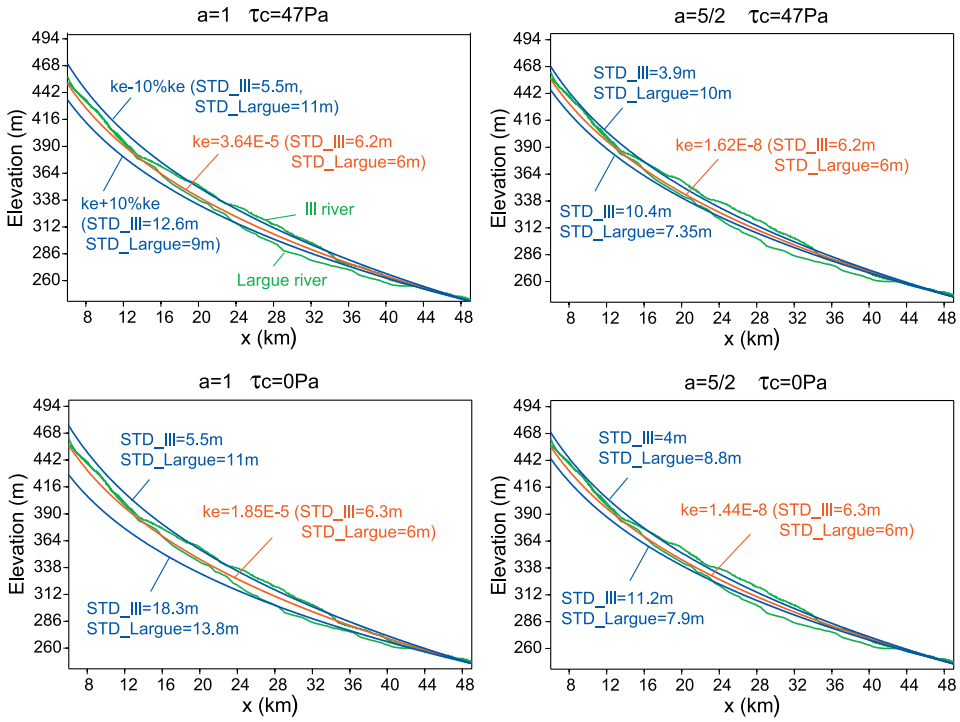

Figure 4. Comparison of Ill and Largue River profiles (green) with models at dynamic equilibrium. The standard deviation (STD) between data and models are indicated in the diagram for each river. The physical parameters used are described in Appendix A. The climate parameters are $\langle P \rangle$ = 500 mm yr^{-1} and F_{var} = 10. The regional uplift rate relative to the pinned bottom boundary is U = 0.1 mm yr^{-1}. The unknown parameter k_e (equation (A1)) is adjusted to fit the fluvial relief (red profile). Two other models (blue profiles) correspond to 10% relative changes in k_e (equation (A1)). This figure shows that the fluvial relief is less sensitive to k_e if $\tau_c > 0$ Pa.

adjust river profiles in this portion, but that is beyond the scope of this study. Moreover, this would not change significantly the profile further downstream because incision depends on the local gradient and drainage area. The best fit dynamic equilibrium profile is obtained by imposing a constant and homogeneous Quaternary regional uplift rate of 0.1 mm yr^{-1} (relative to the pinned bottom boundary) to an initial horizontal profile and by adjusting k_e to fit the fluvial relief. Several climatic scenarii are tested: a constant and homogeneous climate ($\langle P \rangle$ = 500 mm yr^{-1} and F_{var} = 10) and variable climatic conditions.

4.1.1. Constant Climate

[21] Figure 4 shows the observed and modeled profiles for a = 1 and 5/2, and for τ_c = 47 Pa and 0 Pa. The response times to achieve equilibrium are between 2 and 3 My. The adjusted values of k_e are three orders of magnitude lower for a = 5/2 than for a = 1. The STD is given on the graphs and in Table 2. It is around 6 m. In order to evaluate the sensitivity of the fluvial relief to k_e, profiles have been plotted for 10% variations around k_e. This leads to a relative change of the fluvial relief of between 2 and 12% and STD of 3.9 to 18.4 m. The change is smaller for a = 5/2 than for a = 1. The sensitivity significantly differs for τ_c = 47 Pa and 0 Pa if a = 1, but is not significant if a = 5/2. This probably comes from the simplification of the model (equation (A2)) which decreases the effect of τ_c for a = 5/2, as noted in section 3. These results show that a significant threshold value decreases the sensitivity of the relief to k_e.

4.1.2. Varying Climate

[22] In order to evaluate the impact of varying climate on the evolution of river profiles, we vary $\langle P \rangle$ and F_{var} around the mean values of 500 mm yr^{-1} and 10, respectively. Present day data in the United States show that $\langle P \rangle$ and F_{var} vary between an arid pole (low $\langle P \rangle$, high F_{var}) and a humid pole (high $\langle P \rangle$, low F_{var}) [*Tucker*, 2004]). Thus we impose out-of-phase sinusoidal variations of these two parameters to model long-term oscillations of climate during Quaternary times. The tested variations are: periods (T) of 100 ky and 200 ky, phase differences ($d\Phi$) of T/2 and T/4, amplitudes of ±50% and ±90% around the mean values.

[23] Figure 5 shows the resulting profiles after an approximately constant fluvial relief has been achieved (after ~2.2 My for a = 1 and $\tau_c > 0$ Pa and for a = 5/2 and after ~3.5 My for a = 1 and τ_c = 0 Pa). The STD and the adjusted

Table 2. Adjusted k_e of Dynamic Equilibrium Profiles Under Constant and Homogeneous Climate and Uplift[a]

a	τ_c (Pa)	best-fit k_e (m yr^{-1} Pa^{-a})	STD (m)	STD (k_e + 10%k_e)	STD (k_e − 10%k_e)
1	47	3.64 10^{-5}	6.2(I) 6(L)	12.6(I) 9(L)	5.5(I) 11(L)
5/2	47	1.62 10^{-8}	6.2(I) 6(L)	10.4(I) 7.3(L)	3.9(I) 8.5(L)
1	0	1.85 10^{-5}	6.2(I) 6(L)	18.3(I) 13.8(L)	5.5(I) 11(L)
5/2	0	1.44 10^{-8}	6.2(I) 6(L)	11.2(I) 7.9(L)	4(I) 8.8(L)

[a]See Figure 4. (I) refers to the Ill River, and (L) refers to the Largue River. Uplift rates are relative to the pinned bottom condition of river profiles.

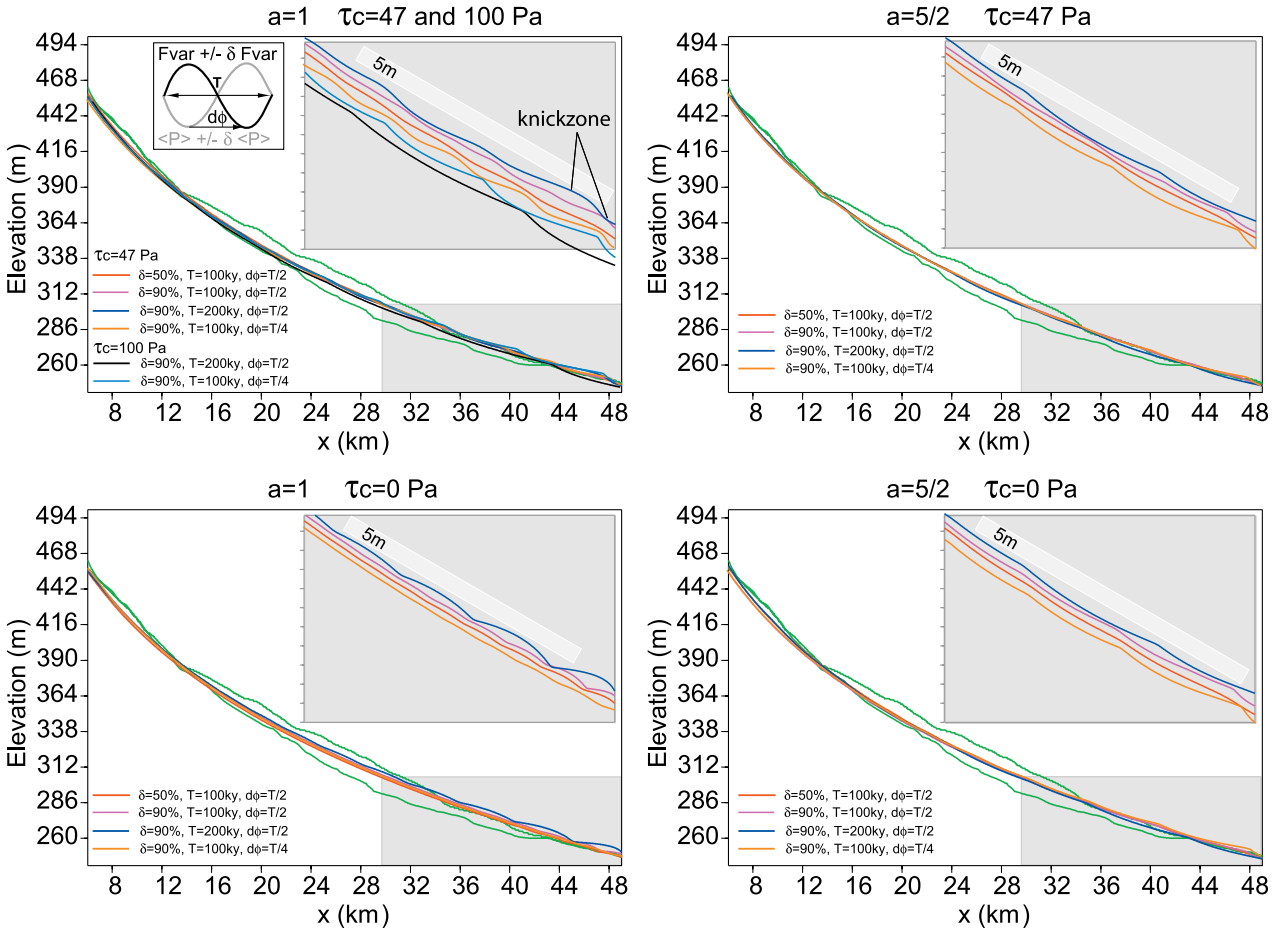

Figure 5. Effect of variable climate. The Ill and Largue profiles are in green. The model profiles are computed by imposing sinusoidal variations to the mean precipitation rate $\langle P \rangle$ and to the variability factor F_{var}. The reference mean values are $\langle P \rangle = 500$ mm yr^{-1} and $F_{var} = 10$ and the constant uplift rate relative to the pinned bottom condition is $U = 0.1$ mm yr^{-1}. The fitting results are given in Table 3. Inset gray diagrams show an enlargement of the last 20 km of the profiles. The profiles have been slightly shifted vertically for ease of viewing. A 5-m ruler is displayed to measure the amplitude of elevation changes because of climate oscillations. These figures show that elevation changes along a single profile are smaller than 5 m whatever the tested scenario and erosion parameters. This suggests that climate variations cannot explain the main knickzone along the Ill River.

values of k_e are given in Table 3. The profiles consist of a system of knickzones which propagate and vanish upstream. The knickzones disappear upstream partly because the finite difference solution tends to smooth any advecting step. A second reason is that deviation from the linear dependence of erosion rate on river gradient ($n \neq 1$ in equation (1), case $\tau_c = 0$ Pa) implies progressive rounding and widening of knickzones [*Whipple*, 2001; *Tucker and Whipple*, 2002]. This is the case in our experiments ($n = 0.67$ for $a = 1$ and $n = 1.67$ for $a = 5/2$). The third reason is that knickzones retreat at a speed that decreases upstream because of the decreasing drainage area and the smoothing of the knickzones [*Gardner*, 1983; *Whipple and Tucker*, 1999]. Thus, as the most upstream knickzones widen and slow, they are overtaken by the following ones and they coalesce. It is interesting to note that the angular or rounded shape of the knickzones is directly linked to how the incision rate evolves with increasing climate variability. Figure 5 and the upper diagrams of Figure 3 show that rounded knickzones correspond to a decreasing incision rate with increasing variability factor F_{var}. This does not depend on the value of a (and thus on the gradient exponent n of the stream power law; see Appendix A), contrary to what is predicted with the classical stream power law without stochastic climate [*Tucker and Whipple*, 2002]. Consequently, the shape of knickzones generated by sinusoidal climate oscillations seems not to be useful for inferring the parameter n of the incision law if the threshold τ_c is significant compared to shear stress at mean climatic conditions.

[24] Knickzones develop at river outlets because the profiles are tectonically advected upwards during low erosion efficiency periods and relax during times of increased erosion efficiency, similarly to river responses to successive base-level changes [*Snyder et al.*, 2002; *Bishop et al.*, 2005]. The relaxation begins at the outlet and propagates upstream as a wave, which is characteristic of the detachment-limited model (equation (1)). Consequently, the change of river bed elevation is mainly controlled by the time period of climatic

Table 3. Adjusted k_e of Models With Variable Climate[a]

a	τ_c, Pa	δ	T, years	dϕ, years	Best Fit k_e, m yr^{-1} Pa^{-a}	STD, m
1	47	50%	10^5	5 10^4	3.64 10^{-5}	5.1(I) 6.5(L)
1	47	90%	10^5	5 10^4	4.44 10^{-5}	6.1(I) 6.3(L)
1	47	90%	2 10^5	10^5	4.44 10^{-5}	5.7(I) 6.9(L)
1	47	90%	10^5	25 10^4	4.79 10^{-5}	5.6(I) 6.7(L)
5/2	47	50%	10^5	5 10^4	1.04 10^{-8}	5.3(I) 6.3(L)
5/2	47	90%	10^5	5 10^4	2.3 10^{-8}	5.7(I) 6.1(L)
5/2	47	90%	2 10^5	10^5	2.24 10^{-8}	6.2(I) 5.3(L)
5/2	47	90%	10^5	25 10^4	1.58 10^{-8}	6(I) 6.3(L)
1	0	50%	10^5	5 10^4	1.75 10^{-5}	6.1(I) 6.4(L)
1	0	90%	10^5	5 10^4	1.35 10^{-5}	5.2(I) 7.3(L)
1	0	90%	2 10^5	10^5	1.35 10^{-5}	4.3(I) 9.(L)
1	0	90%	10^5	25 10^4	1.75 10^{-5}	6.5(I) 5.8(L)
5/2	0	50%	10^5	5 10^4	1.48 10^{-8}	5.4(I) 6.3(L)
5/2	0	90%	10^5	5 10^4	1.89 10^{-8}	6.6(I) 6.2(L)
5/2	0	90%	2 10^5	10^5	2.5 10^{-8}	6.1(I) 5.2(L)
5/2	0	90%	10^5	25 10^4	1.42 10^{-8}	6.6(I) 6.2(L)
1	100	90%	2 10^5	10^5	2.25 10^{-4}	6.5(I) 5.8(L)
1	100	90%	10^5	25 10^4	1.12 10^{-4}	6.4(I) 6.5(L)

[a]See Figure 5. T is the period of climate oscillation, and dϕ is the difference of phase between variations of the mean precipitation rate $\langle P \rangle$ and of the variability factor F_{var} (see Figure 5). (I) refers to the Ill River, and (L) refers to the Largue River.

oscillations, as shown by the greater amplitudes obtained with the 200 ky periods. Considering zero erosion during the low efficiency half period $T/2$ of the climatic cycle, the product of the uplift rate and $T/2$ gives an upper bound to the possible river incision of between 5 and 10 m. These values correspond to the difference of relief between two equilibrium profiles, a low one corresponding to the high erosion conditions and a higher one corresponding to the low erosion conditions [*Whipple*, 2001]. With larger variations of mean precipitation rate $\langle P \rangle$, the first profile could be less elevated (because mean erosion rate $\langle E \rangle$ increases with $\langle P \rangle$; see Figure 3) but the height difference could not exceed 5–10 m above it. To sum up, the maximum possible change of river bed elevation does not depend on the mean precipitation rate variations.

[25] Despite their differences, the models predict changes of river bed elevation changes which are less than 5 m, which is much smaller than the knickzone amplitude of the Ill profile (Figure 2a). Furthermore, the persistence of successive knickzones shows that the response time of the river to climatic variations is much greater than the imposed time periods of oscillations, as already demonstrated in the case of the stream power law model [*Whipple*, 2001]. This prevents the occurrence of significant incision along the whole profile during periods of high erosional efficiency. Small predicted variations in river bed elevation suggest that climate variations have limited impact on the studied profiles.

4.2. Perturbation by Localized Uplift

[26] We now test the hypothesis that the knickzones above folds are due to local uplift. We start from dynamic equilibrium profiles with constant climate, and we add box-like uplift patterns at the locations of the highest anticlines along the Ill River (the Altkirch anticline, at ~33 km) and Largue River (the Dannemarie anticline at ~25 km). The other smaller anticlines have not been modeled because we are interested in the first order response of the river to the tectonic perturbation. On the Largue River, we also decrease the uplift rate between the Dannemarie and Illfurth anticlines, a reach where the regional rock uplift rate relative to Mulhouse is probably lower [*Nivière and Winter*, 2000]. We perform a parameter search procedure to calculate best fit values of the added or subtracted uplift. The best fit value corresponds to the minimum of the STD (root mean square inversion). The fitting procedure includes also the time span after the onset of anticline growth (the age of the anticline).

[27] Figure 6 displays model results for the two rivers and for the case $\tau_c = 47$ Pa and $a = 1$. In the case of the Ill River, a new equilibrium profile develops from the anticline (U1) and propagates upstream. A knickzone appears above the anticline and remains fixed. The profile is progressively uplifted vertically above it and upstream. In the case of the Largue River, the profile is uplifted above the Dannemarie fold (U2) and then subsides because of the lower uplift rate downstream (U3). The best fit profiles account for the knickzone in the Ill River near km 33 and for the steeper reach of the Largue profile around km 25. The fit between profiles is better than fits obtained in previous sections (STD is between 1 and 2 m, compared to 6 m for initial equilibrium profiles). Moreover, the product of uplift rates and best fit age predict cumulative uplifts consistent with the fold amplitude of the base of the Sundgau Gravels (~50 m, Figure 1b). The inset diagram of Figure 6a shows that the curves of STD versus anticline age are roughly flat after ~1 My for the Ill profile. This is because the transient wave has propagated to the upper edge of the model space. This suggests that the Ill River has reached a new equilibrium, at least in the studied reach. For the Largue River, the curve of STD versus anticline age shows a minimum. The goodness of fit decreases with increasing ages. This suggests that the Largue profile corresponds to a transient profile adjusting to local uplift rate perturbation. The predicted ages (minimum age for the Ill River) for the onset of anticline growth are similar for the two rivers (~1 My).

[28] The behavior of these transient rivers and the resulting fits are very similar for different values of τ_c and a (Table 4). The only differences are (1) the more or less rounded shape of the knickzones which is a second-order observation given the simplified form of the imposed tectonic uplift, (2) the response time, and (3) the adjusted uplift rates. Only the best fit response times vary significantly (between 0.65 and 2.1 My), but even added to the time required to achieve a first dynamic equilibrium (~2 My), these remain consistently lower than the upper bound age of the Sundgau Gravels (between 2.6 and 4.2 My). Without further constraints on the age of anticline growth, it is not possible to decide between the tested models, which all appear equally good.

5. Discussion

5.1. Effect of Uplift Rate

[29] The main conclusion of our study is that climate change over the Quaternary may have had minor effects on the evolution of the two river profiles compared to those of anticline growth, even though the rock uplift rate is low. This arises from two common outcomes of the tested detachment-limited models: (1) Elevation change cannot exceed the rock uplift during low erosion efficiency periods, and (2) the incision during high erosion efficiency periods

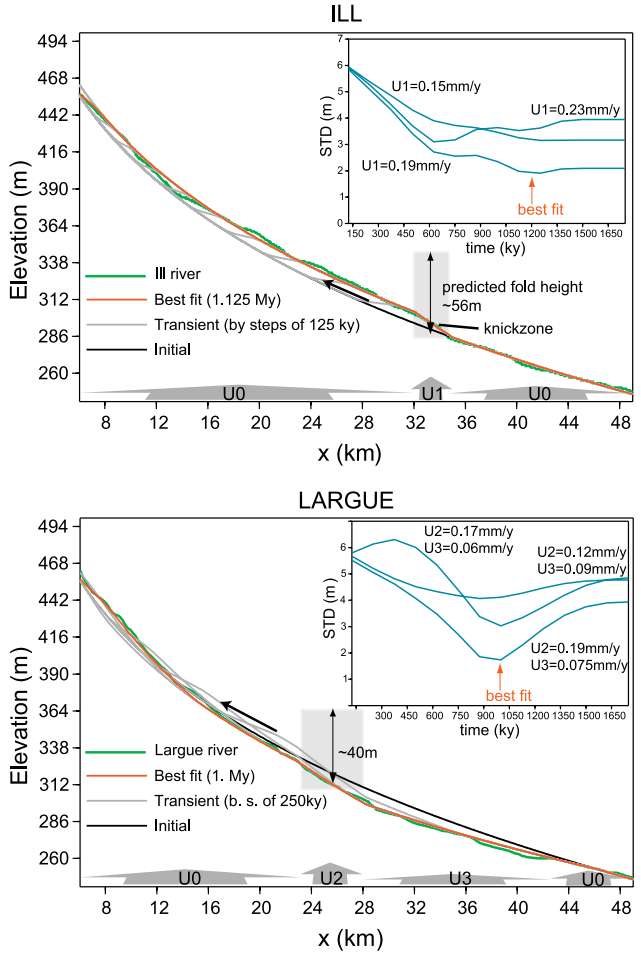

Figure 6. Effect of local uplift. An initial dynamic equilibrium (black profile) has been assumed for the (top) Ill and (bottom) Largue profiles (green) with an uplift rate of $Uo = 0.1$ mm yr^{-1} relative to the pinned bottom condition. Then increased (or decreased) rock uplift rates have been imposed at the locations of anticlines and where the Largue River flows out of the main uplifted region. The red profiles correspond to the best fit profiles among models with different local uplift rates and time spans since the onset of additional uplift. Gray profiles correspond to transient profiles computed for best fit uplift rates. For the Ill River, a new equilibrium profile develops starting from the location of the increased local uplift and then propagates headward (gray profiles). A knickzone develops above U1 and remains fixed, as shown by the gray profiles which are successive transient profiles. For the Largue profile, transient stages show a first uplift of the profile above U2 and then the profile subsides. The STD versus time (inset diagrams) decreases and flattens for the Ill River. This suggests that the observed profile corresponds to a new equilibrium, at least in the studied reach. For the Largue River, the curve of the STD shows a minima corresponding to the best fit profile. This suggests that the observed profile corresponds to a transient profile. The predicted fold heights (gray boxes) correspond to the difference between cumulative local and regional uplifts. They correspond to the order of magnitude of folds at the base of the Sundgau Gravels base (50–100 m). The parameters used in this models are $a = 1$, $\tau_c = 47$ Pa, $\langle P \rangle = 500$ mm yr^{-1}, and $F_{var} = 10$.

cannot propagate far upstream because the response time of the river is too long compared to the timescale of climatic oscillations. The first limitation is set up by the low regional uplift rate U. Higher rock uplift rates should allow larger climate-induced profile variations. To illustrate this, we plot in Figure 7 different profiles obtained by changing k_e or U by a factor of 10. For a given fluvial relief, greater profile variations occur for greater uplift rate. In these cases, climate-driven variations of river bed elevation are more likely to obscure spatial variations of the uplift rate, although this should depend obviously on the magnitude of these variations and on the distance of local uplift relative to the base level.

[30] The impact of U on climate-induced elevation change can be shown analytically in the case of nonstochastic rainfall and negligible τ_c (stream power law model). The maximum possible elevation change can be defined as the difference of fluvial relief between two equilibrium profiles, corresponding to two differing climate or tectonic conditions. *Whipple and Tucker* [1999] have shown that the stream power law predicts that the dynamic equilibrium relief R scales as

$$R \propto P^{-\frac{m}{n}} U^{\frac{1}{n}}, \tag{4}$$

where P represents a mean precipitation rate. Taking the log derivative, we can express the relationship between fractional changes of R, P and U [*Roe et al.*, 2006].

$$\frac{dR}{R} = -\frac{m}{n}\frac{dP}{P} + \frac{1}{n}\frac{dU}{U}. \tag{5}$$

This shows that relief change is greater for an uplift rate change than for a precipitation rate for an identical amount of relative change of both parameters, and for classical values of $\frac{m}{n} = 0.5$ and $n < 2$. If U is constant, then

$$dR = -U^{\frac{1}{n}}\frac{m}{n}\frac{dP}{P}P^{-\frac{m}{n}}. \tag{6}$$

This means that the climate-induced relief variations are greater for larger uplift rates. *Snyder et al.* [2003a] and *Tucker* [2004] showed that the relationship between R and U is weaker for large uplift rates than for low uplift rates if $\tau_c > 0$ Pa and for a Poisson distribution of floods. *Lague et al.* [2005] demonstrated also a weaker relationship between relief and increasing high uplift rates by using a frequency-magnitude distribution of discharge characterized by a "heavy" tail, with power-law scaling of the probability density function of floods. This reinforces our conclusion because increase of high uplift rate will produce a relatively smaller relief increase than that produced by increase of a low uplift rate. Thus tectonic knickpoints and knickzones are even more likely to dominate those generated during climatic variations for low uplift rate than for high uplift rate. We note, however, that this is valid only for a pinned lower boundary condition, as imposed in our experiments. If the boundary condition corresponds to a strong contrast between the detachment-limited uplifted domain and a transport-limited alluvial plain, differential erosion at the transition can produce a local base-level fall which propagates upstream as a knickzone [*Carretier and Lucazeau*, 2005], possibly removing uplift signatures above faults and folds. Similarly, climatic

Table 4. Adjusted Parameter Values of Models With Additional Uplift[a]

			Best Fit Values						
a	τ_c, Pa	k_e, m yr^{-1} Pa^{-a}	U1(I), mm yr^{-1}	U2(L), mm yr^{-1}	U3(L), mm yr^{-1}	Anticline Age, years		STD, m	
1	47	3.64 10^{-5}	0.19	0.14	0.075	1.2 10^6(I)	10^6(L)	2.8(I)	1.7(L)
5/2	47	1.62 10^{-8}	0.3	0.19	0.063	0.9 10^6(I)	0.65 10^6(L)	2(I)	1.9(L)
1	0	1.85 10^{-5}	0.15	0.125	0.085	2.1 10^6(I)	1.7 10^6(L)	1.8(I)	1.4(L)
5/2	0	1.44 10^{-8}	0.27	0.19	0.063	10^6(I)	0.7 10^6(L)	2.(I)	2.(L)

[a]See Figure 6 for the location of zones with uplift rates U1, U2 and U3. (I) refers to the Ill River and (L) to the Largue River.

sea-level fluctuations at river outlets can generate migrating knickzones [*Snyder et al.*, 2002; *Bishop et al.*, 2005]. Moreover, the limited climatic incision is strongly controlled by the regional uplift relative to the pinned outlet boundary condition. Without regional uplift, climatic incision could be greater during high erosion periods, and it could affect the whole river profile [e.g., *Zaprowski et al.*, 2005], possibly removing local uplift signatures.

5.2. Limitations of the Model

[31] The first limitation of the tested detachment-limited models is that they can only predict incision, and not deposition. This is a strong limitation for predicting variations of river bed elevation when climate varies. In particular, the model can not account for back limb sedimentation if the gradient is reversed behind folds (which does not occur in these experiments). It is very likely that deposition and transport-limited conditions occurred during Quaternary times, and it is possible that erosion shifted toward detachment-limited conditions only because of anticline uplift [*Whipple and Tucker*, 2002]. For example, the Sundgau Gravels are overlain by a discontinuous Wurmian loess cover [e.g., *Vogt*, 1992] whose thickness is less than 20 m. These deposits should have covered the entire drainage network and their removal may have been transport-limited. However, neglecting transport-limited periods should not affect our conclusion that climatic induced knickzones are less important than those generated by differential rock uplift. Indeed, deposition usually smoothes variations of river gradients. Therefore neglecting deposition with detachment-limited models should predict the highest elevation changes. On the other hand, assuming constant detachment limited conditions underestimates the response times because periods of transport-limited conditions are not taken into account. However, even underestimated, response times associated with climate induced knickzones migration are still greater than imposed climatic variations, which explains why knickzones are observed in synthetic profiles. Thus underestimation of response time should not affect our conclusions.

[32] Model response times are likely to be modified by other time-dependent processes that have been neglected here, such as time variations of τ_c due to variation of the vegetation cover, variation of at-a-station river width geometry (k_w and s in equation A7) during the incision of different rock types and because of local uplift and variation of runoff because of infiltration variations. Variation of abrasion efficiency because of variable rate of gravel supply may also have had a significant impact on river response times. We tested two end-member models which may be correct for bedrock abrasion: a model with an excess shear stress dependence more than linear (a = 5/2, [*Whipple et al.*, 2000]), and a model with a = 1, which may be consistent, as suggested by *Lague et al.* [2005], with a recent model of abrasion by saltation proposed by *Sklar and Dietrich* [2004]. However, *Sklar and Dietrich* [2004] have clearly shown that their model should imply variations of the erosional efficiency coefficient k_e (equation (A1)) along the river profile and through time, which has not been taken into account in our study. The different values of a led to similar river responses but with very different response times to local increased uplift. This difference may be greater with temporal variations of k_e. The evaluation of consequences of variable k_e and the difference in predicted response times may be used to test the values of a. In our study, it was not possible to do this because of the uncertainty on the ages of anticline growth.

6. Conclusion

[33] Our study suggests that long-term climate variations have not significantly affected the studied river profiles when compared with differential rock uplift across growing anticlines. This results from two assumptions: (1) the long-

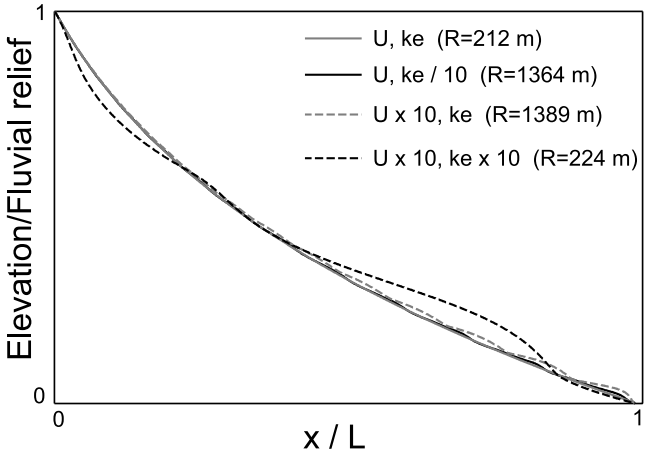

Figure 7. Effect of regional rock uplift rate U on the height of knickzones generated during low erosion efficiency of climate variations. The bottom boundary is pinned. Model profiles are scaled by their fluvial relief and their length. Climate variations correspond to sinusoidal oscillations (100 ky period) of the mean precipitation rate $\langle P \rangle$ and of the variability factor F_{var} around 500 mm yr^{-1} and 10, respectively. These two sinusoids have amplitude of 90% of their mean, and they are out of phase. The reference uplift rate U relative to the pinned lower boundary is 0.1 mm yr^{-1} and $k_e = 4.44 \times 10^{-5}$ m yr^{-1} Pa^{-1} (a = 1, τ_c = 47 Pa). The fluvial relief is as large as the erosion efficiency parameter k_e (equation (A2)) is small. This figure shows that along-profile variations because of climate oscillation are greater for large uplift rates, and that this difference is much greater for low-relief rivers than for high-relief rivers.

Table A1. Model Parameters

ϵ [L T^{-1}]	rate of channel incision (equation (A1))
τ [M L^{-1} T^{-2}]	average bed shear stress (equation (A1))
τ_c [M L^{-1} T^{-2}]	critical detachment shear stress (equation (A1))
k_e [M^{-a} L^{1+a} T^{-1+2a}]	incision efficiency factor (equation (A1))
a	exponent in the incision rate relationship (equation (A1))
Q [L^3 T^{-1}]	water discharge (equation (A3))
S	river gradient (equation (A3))
w [L]	river width (equation (A3))
k_t [M L$^{-2\alpha-1}$ T$^{\alpha-2}$]	factor in the friction law (equations (A3), (A4), and (A5))
α	exponent of water discharge per unit width in the friction law (equation (A3))
β	exponent of river gradient in the friction law (equation (A3))
ρ [M L^{-3}]	flow density (equation (A4))
f	Darcy friction factor (equation (A4))
g [L T^{-2}]	gravitational acceleration (equation (A4))
N	Manning friction factor (equation (A5))
R [L T^{-1}]	runoff (equation (A6))
A [L^2]	drainage area (equation (A6))
k_w [L^{1-3b} T^b]	factor in the width-discharge power law (equation (A7))
b	exponent in the downstream hydraulic geometry power law (equation (A7))
Q_m [L^3 T^{-1}]	mean water discharge (equation (A8))
w_m [L]	river width for mean discharge condition (equation (A8))
s	exponent in the at-station hydraulic geometry relationship (equation (A8))
R_m [L T^{-1}]	mean runoff (equation (A9))
$\langle E \rangle$ [L T^{-1}]	mean rate of channel incision (equation (A10))
K_R [L$^{1+3a\alpha(b-1)}$ T$^{-1+a\alpha(1-b)}$]	threshold factor in the stochastic threshold model equation (A10))
K_C [L$^{a\alpha(1-b)}$ T$^{-a\alpha(1-b)}$]	climate factor in the stochastic threshold model (equation (A10))
I [L T^{-1}]	infiltration rate (equation (A15))
P [L T^{-1}]	precipitation rate of a rainfall event (equation (A15))
$\langle P \rangle$ [L T^{-1}]	mean precipitation rate (equation (A15))
m	drainage area exponent in the stochastic threshold model (equation (A10))
n	gradient exponent in the stochastic threshold model (equation (A10))
F_{var}	variability factor (equations (A15) and (A17))

term incision process has been detachment-limited, and (2) the regional uplift rate has been small but greater than zero. The conclusion is the opposite for relaxing rivers and for rivers uplifted at a high rate, and it would be probably different for transport-limited rivers. The tested models (with or without threshold, a = 1 or 5/2) led to similar transient responses to tectonic and climatic perturbations, but with different response times, which appears to be a critical parameter to decipher between model parameter values. It has not been possible to reject models from their different predicted response times because the precise ages of anticline onset are not known. The predicted transient profiles are in good agreement with the observed ones, suggesting that the detachment-limited models are appropriate to this case. Despite a lot of uncertainties about model assumptions, the similar results obtained with the tested models suggest that such modeling approach can improve the detection and the quantification of active structures in low uplift rate environments.

Appendix A: Stochastic Threshold Model

A1. Averaged Incision Rate Model

[34] The model is briefly described here. The details are given by *Tucker and Bras* [2000] and *Tucker* [2004]. Parameters and their dimension are also defined in Table A1.

[35] Erosion rate ϵ [L T^{-1}] during a storm event is assumed to be [*Tucker and Bras*, 2000; *Tucker*, 2004; *Snyder et al.*, 2003a, 2003b]

$$\epsilon = k_e(\tau - \tau_c)^a, \tag{A1}$$

where τ and τ_c [M L^{-1} T^{-2}] are shear stress and critical shear stress for detachment, respectively. Equation (A1) is simplified into the following form to make an analytical solution tractable for stochastic climate:

$$\epsilon = k_e\left(\tau^a - \tau_c^a\right). \tag{A2}$$

[36] The shear stress is expressed as

$$\tau = k_t\left(\frac{Q}{w}\right)^{\alpha} S^{\beta}, \tag{A3}$$

where Q [L^3 T^{-1}] is the water discharge, w [L] the river width and S the river gradient.

[37] Empirical relations are as follows. If the Darcy-Weisbach law is used,

$$k_t = 1/2\ \rho\ g^{2/3} f^{1/3}, \tag{A4}$$

and if the Manning law is used,

$$k_t = \rho\ g N^{3/5}, \tag{A5}$$

where g [L T^{-2}] is the gravitational acceleration, ρ [M L^{-3}] the density and f and N are friction coefficients.

Discharge-drainage area (R [L T^{-1}] is the runoff, A [L^2] is the drainage area),

$$Q = R\ A. \tag{A6}$$

Width-discharge is

$$w = k_w Q^b. \tag{A7}$$

At-station width-discharge (the mean discharge Q_m [$L^3\ T^{-1}$] and the related river width w_m [L] are taken as reference) is

$$w/w_m = (Q/Q_m)^s. \tag{A8}$$

[38] "Mean" discharge-runoff (R_m [$L\ T^{-1}$]) is runoff for mean discharge) is

$$Q_m = R_m A. \tag{A9}$$

[39] The stochastic threshold model for mean incision rate $\langle E \rangle$ [$L\ T^{-1}$]) is

$$\langle E \rangle = K_R K_C K_{\tau c}\ A^m S^n, \tag{A10}$$

where

$$m = \alpha a (1 - b), \tag{A11}$$

$$n = a\beta, \tag{A12}$$

$$K_R = k_e k_w^{-\alpha a} k_t^a, \tag{A13}$$

$$K_C = F_{var}^{\gamma_b - 1} \langle P \rangle^{\gamma_b} R_m^{-\epsilon_b} \exp\left(-\frac{I}{P}\right) \Gamma(\gamma_b + 1), \tag{A14}$$

$$K_{\tau c} = \frac{\Gamma\left(\gamma_b + 1, \frac{R_c}{P}\right) - \left(\frac{R_c}{P}\right)^{\gamma_b} \exp\left(-\frac{R_c}{P}\right)}{\Gamma(\gamma_b + 1)}, \tag{A15}$$

$$R_c = \left(\tau_c k_t^{-1} R_m^{a(b-s)} k_\omega^{\alpha} A^{-\alpha(1-b)} S^{-\beta}\right)^{\frac{1}{\alpha(1-\omega)}}, \tag{A16}$$

$$F_{var} = P/\langle P \rangle, \tag{A17}$$

$$\gamma_b = \alpha a (1 - s), \tag{A18}$$

$$\epsilon_b = \alpha a (b - s). \tag{A19}$$

$\langle P \rangle$ [$L\ T^{-1}$] is the mean precipitation rate. P [$L\ T^{-1}$] is the instantaneous precipitation rate of a rainfall event. I [$L\ T^{-1}$] is the infiltration rate. F_{var} is called the variability factor. $\Gamma(,)$ is the incomplete Gamma function. Note that $K_{\tau c}$ depends on the gradient S and drainage area A.

A2. Parameter Values

[40] The parameter k_t (equations (A3), (A4) and (A5)) is estimated to be 1.33×10^{-2} Pa $m^{-1.3} yr^{0.67}$ with the Darcy-Weisbach relationship (water with suspended load density ρ = 1400 kg m^{-3}, gravitational acceleration g = 9.81 m s^{-2}, roughness parameter f = 0.08 for gravel-cobble bed) and 1.4×10^{-2} Pa $m^{-1.3} yr^{0.6}$ with the Manning relationship (roughness N = 0.03 for gravel bed). Both values do not change our results significantly when combined with corresponding values of α (2/3 with Darcy-Weisbach and 3/5 with Manning) and β (2/3 with Darcy-Weisbach and 7/10 with Manning). The Darcy-Weisbach parameters are used for the calculations.

[41] The width-discharge relation (equation (A7)) is calibrated using the classical exponent b = 0.5 [*Leopold and Maddock*, 1953]; [*Montgomery and Gran*, 2001] and taking $k_w = 0.4 \times 10^{-3}$ $m^{-0.5}$ $yr^{0.5}$ to obtain a river width of about 4 m at 35 km for mean discharge conditions.

[42] Mean at-station discharge Q_m in the at-station width-discharge relation (equation (A8)) is evaluated using a mean precipitation rate $\langle P \rangle$ = 500 mm yr^{-1} and a mean infiltration rate $\langle I \rangle$ = 250 mm yr^{-1} averaged over 30 years and over an area of 50 km × 50 km centered on the Sundgau area. The geometrical exponent s is taken as 0.25, which corresponds to a concave channel section.

[43] Consequently, if a = 1 then γ_b = 0.5, ϵ_b = 0.167, n = 0.67, m = 0.335 and if a = 5/2 γ_b = 1.25, ϵ_b = 0.42, n = 1.67, and m = 0.84. The remaining parameters (F_{var}, k_e, τ_c) are discussed in section 3.

[44] **Acknowledgments.** We thanks F. J. Pazzaglia, P. L. K. Knuepfer, and an anonymous reviewer for their help in improving a previous version of this paper. We are grateful to J.-C. Soula, V. Regard, and M. Jessell for manuscript corrections. We thank R. Anderson, P. Bishop, N. Snyder, and A. Densmore for very helpful reviews which improved greatly our manuscript. A. Densmore very much improved the writing. Part of this work was supported financially by the European project SAFE (Slow Active Fault in Europe, project EVG1-2000-22005) supervised by M. Sébrier.

References

Allen, P. A., and A. L. Densmore (2000), Sediment flux from an uplifting fault block, *Basin Res.*, *12*, 367–380.

Arrowsmith, J. R., D. D. Pollard, and D. D. Rhodes (1996), Hillslope development in areas of active tectonics, *J. Geophys. Res.*, *101*, 6255–6275.

Bishop, P., T. B. Hoey, J. D. Jansen, and I. L. Artza (2005), Knickpoint recession rate and catchment area: The case of uplifted rivers in eastern Scotland, *Earth Surf. Processes Landforms*, *30*, 767–778, doi:10.1002/esp.1191.

Brocard, G., and P. A. van der Beek (2006), Influence of incision rate, rock strength and bedload supply on bedrock river gradients and valley-flat widths: Field-based evidence and calibrations from western alpine rivers (SE France), in *Tectonics, Climate and Landscape Evolution*, edited by S. D. Willett et al., *Spec. Pap. Geol. Soc. Am.*, in press.

Camelbeeck, T., and M. Meghraoui (1998), Geological and geophysical evidence for large palaeo-earthquakes with surface faulting in the Roer Graben (northwest Europe), *Geophys. J. Int.*, *132*, 347–362.

Carretier, S., and F. Lucazeau (2005), How does alluvial sedimentation at range fronts modify the erosional dynamics of mountain catchments?, *Basin Res.*, *17*, 361–381, doi:10.1111/j.1365-2117.2005.00270.x.

Carretier, S., J.-F. Ritz, A. Bayasgalan, and J. Jackson (2002), Morphological dating of cumulative reverse fault scarp, example of the Gurvan Bogd Range, Mongolia, *Geophys. J. Int.*, *148*, 256–277.

Cox, R. (1994), Analysis of drainage basin symmetry as a rapid technique to identify areas of possible Quaternary tilt-block tectonics: An example from the Mississippi embayment, *Geol. Soc. Am. Bull.*, *106*, 571–581.

Crave, A., and P. Davy (2001), A stochastic "precipitation" model for simulating erosion/sedimentation dynamics, *Comput. Geosci.*, *27*(7), 815–827.

Dèzes, P., S. Schmid, and P. Ziegler (2004), Evolution of the European Cenozoic Rift System: Interaction of the Alpine and Pyrenean orogens with their foreland lithosphere, *Tectonophysics*, *389*, 1–33, doi:10.1016/j.tecto.2004.06.011.

Fejfar, O., W.-D. Heinrich, and E. Lindsay (1998), Updating the Neogene rodent biochronology in Europe, *Meded. Ned. Inst. Toegepaste Geowetensch.*, *60*, 533–554.

Gardner, T. W. (1983), Experimental study of knickpoint and longitudinal profile evolution in cohesive, homogeneous material, *Geol. Soc. Am. Bull.*, *94*, 664–672.

Gaudemer, Y., P. Tapponier, and D. Turcotte (1989), River offsets across active strike-slip faults, *Ann. Tecton.*, *III*, 55–76.

Giamboni, M., K. Ustaszewski, S. M. Schmid, M. E. Schumacher, and A. Wetzel (2004a), Plio-Pleistocene transpressional reactivation of Paleozoic and Paleogene structures in the Rhine-Bresse transform zone (northern Switzerland and eastern France), *Int. J. Earth Sci.*, *93*, 207–223, doi:10.1007/s00531-003-0375-2.

Giamboni, M., A. Wetzel, B. Nivière, and M. Schumacher (2004b), Plio-Pleistocene folding in the southern Rhine Graben recorded by the evolution of the drainage network (Sundgau area, northwestern Switzerland and France, *Eclogea Geol. Helv.*, *97*, 17–31.

Giamboni, M., A. Wetzel, and B. Schneider (2005), Geomorphic response of alluvial rivers to active tectonics: Example from the southern Rhine Graben, *Aust. J. Earth Sci.*, *97*, 24–37.

Hack, J. T. (1973), Stream-profile analysis and stream-gradient index, *J. Res. U.S. Geol. Surv.*, *1*, 421–429.

Hanks, T. C. (1999), The age of scarplike landforms from diffusion-equation analysis, in *Quaternary Geochronology: Methods and Applications*, *AGU Ref. Shelf*, vol. 4, edited by J. S. Noller, J. M. Sowers, and W. R. Lettis, pp. 313–338, AGU, Washington, D. C.

Hodges, K. V., C. Wobus, K. Ruhl, T. Schildgen, and K. Whipple (2004), Quaternary deformation, river steepening, and heavy precipitation at the front of the Higher Himalayan ranges, *Earth Planet. Sci. Lett.*, *220*, 379–389.

Howard, A. D., W. E. Dietrich, and M. A. Seidl (1994), Modeling fluvial erosion on regional to continental scales, *J. Geophys. Res.*, *99*, 13,971–13,986.

Hurtrez, J.-E., F. Lucazeau, J. Lavé, and J.-P. Avouac (1999), Investigation of the relationships between basin morphology, tectonic uplift, and denudation from the study of an active fold belt in the Siawlik hills, central Nepal, *J. Geophys. Res.*, *104*, 12,779–12,796.

Jackson, J., R. Noris, and J. Youngson (1996), The structural evolution of active fault and fold systems in central Otago, New Zealand: Evidence revealed by drainage patterns, *J. Struct. Geol.*, *18*, 217–234.

Kirby, E., and K. X. Whipple (2001), Quantifying differential rock-uplift rates via stream profile analysis, *Geology*, *29*, 415–418.

Krzyszkowski, D., B. Przybylski, and J. Badura (2000), The role of neotectonics and glaciation on terrace formation along the Nysa Klodzka River in the Sudeten Mountains southwestern Poland, *Geomorphology*, *33*, 149–166.

Lague, D., P. Davy, and A. Crave (2000), Estimating uplift rate and erodability from the area-slope relationship: Examples from Brittany (France) and numerical modelling, *Phys. Chem. Earth*, *25*, 543–548.

Lague, D., N. Hovius, and P. Davy (2005), Discharge, discharge variability, and the bedrock channel profile, *J. Geophys. Res.*, *110*, F03004, doi:10.1029/2004JF000138.

Laubscher, H. (2001), Plate interactions at the southern end of the Rhine Graben, *Tectonophysics*, *343*, 1–19.

Lavé, J., and J.-P. Avouac (2000), Active folding of fluvial terraces across the Siwalik Hills, Himalayas of central Nepal, *J. Geophys. Res.*, *105*, 5735–5770.

Lavé, J., and J.-P. Avouac (2001), Fluvial incision and tectonic uplift across the Himalayas of central Nepal, *J. Geophys. Res.*, *106*, 26,561–26,591.

Leopold, L. B., and T. J. Maddock (1953), The hydraulic geometry of stream channels and some physiographic implications, *U.S. Geol. Surv. Prof. Pap.*, *252*, 57 pp.

Maddy, D., D. Bridgland, and C. Green (2000), Crustal uplift in southern England: Evidence from the river terrace records, *Geomorphology*, *33*, 167–181.

McGill, S., and K. Sieh (1991), Surficial offsets on the central and eastern Garlock fault associated with prehistoric earthquakes, *J. Geophys. Res.*, *96*, 21,597–21,621.

Merritts, D. J., K. R. Vincent, and E. E. Wohl (1994), Long river profiles, tectonism, and eustasy: A guide to interpreting fluvial terraces, *J. Geophys. Res.*, *99*, 14,031–14,050.

Meyer, B., Y. Lacassin, J. Brulhet, and B. Mouroux (1994), The Basel 1356 earthquake: Which fault produced it?, *Terra Nova*, *11*, 54–63.

Molnar, P. (2001), Climate change, flooding in arid environments, and erosion rates, *Geology*, *29*, 1071–1074.

Molnar, P., et al. (1994), Quaternary climate change and the formation of river terraces across growing anticlines on the north flank of the Tien Shan, *China, J. Geol.*, *102*, 583–602.

Montgomery, D. R., and W. E. Gran (2001), Downstream variations in the width of bedrock channels, *Water Resour. Res.*, *37*(6), 1841–1846.

Nivière, B., and T. Winter (2000), Pleistocene northwards fold propagation of the Jura within the southern Upper Rhine Graben: Seismotectonic implications, *Global Planet. Change*, *27*, 263–288.

Nivière, B., M. Giamboni, C. Innocent, and T. Winter (2006), Kinematic evolution of a tectonic wedge above a flat-lying decollement: The Alpine foreland at the interface between the Jura Mountains (northern Alps) and the Upper Rhine Graben, *Geology*, in press.

Ouchi, S. (1985), Response of alluvial rivers to slow active tectonic movement, *Geol. Soc. Am. Bull.*, *96*, 504–515.

Pazzaglia, F. J., and M. T. Brandon (2001), A fluvial record of long-term steady state uplift and erosion across the Cascadia forearc high, western Washington State, *Am. J. Sci.*, *301*, 385–431.

Petit, C., M. Campy, J. Chaline, and J. Bonvalot (1996), Major palaeohydrographic changes in Alpine foreland during the Pliocene-Pleistocene, *Boreas*, *25*, 131–143.

Poisson, B., and J.-P. Avouac (2004), Holocene hydrological changes inferred from alluvial stream entrenchment in north Tian Shan (northwestern China), *J. Geol.*, *112*, 231–249, doi:0022-1376/2004/11202-0006.

Ritz, J. F., et al. (2003), Analysing the uplift rate along the Gurvan Bulag thrust fault (Gobi-Altay, Mongolia) during the last 130,000 yrs from ^{10}Be dates: Consequence in terms of seismic activity, *J. Geophys. Res.*, *108*(B3), 2162, doi:10.1029/2001JB000553.

Rockwell, T., E. Keller, M. Clark, and D. Johnson (1984), Chronology and rates of faulting of Ventura river terraces, California, *Geol. Soc. Am. Bull.*, *95*, 1466–1474.

Roe, G. H., D. Stolar, and S. Willett (2006), The sensitivity of a critical wedge orogen to climatic and tectonic forcing, in *Tectonics, Climate and Landscape Evolution*, edited by S. D. Willett et al., *Geol. Soc. Am. Spec. Publ.*, in press.

Rosenbloom, N. A., and R. S. Anderson (1994), Hillslope and channel evolution in a marine terraced landscape, Santa Cruz, California, *J. Geophys. Res.*, *99*, 14,013–14,029.

Schumacher, M. E. (2002), Upper Rhine Graben: Role of preexisting structures during rift evolution, *Tectonics*, *21*(1), 1006, doi:10.1029/2001TC900022.

Seeber, L., and V. Gornitz (1983), River profiles along the Himalayan arc as indicators of active tectonics, *Tectonophysics*, *92*, 335–367.

Siame, L., D. L. Bourlès, M. Sébrier, O. Bélier, J. C. Castano, M. Araujo, M. Perez, G. M. Raisebeck, and F. You (1997), Cosmogenic dating ranging from 20 to 700 ka of a series of alluvial fan surfaces by the El Tigre fault, Argentina, *Geology*, *25*, 975–978.

Sissingh, W. (1998), Comparative tertiary stratigraphy of the Rhine Graben, Bresse Graben and molasse basin: Correlation of Alpine foreland events, *Tectonophysics*, *300*, 249–284.

Sklar, L. S., and W. E. Dietrich (2004), A mechanistic model for river incision into bedrock by saltating bed load, *Water Resour. Res.*, *40*, W06301, doi:10.1029/2003WR002496.

Snyder, N. P., K. X. Whipple, G. E. Tucker, and D. J. Merritts (2002), Interactions between onshore bedrock-channel incision and nearshore wave-base erosion forced by eustasy and tectonics, *Basin Res.*, *14*, 105–127.

Snyder, N. P., K. X. Whipple, G. E. Tucker, and D. J. Merritts (2003a), Importance of a stochastic distribution of floods and erosion thresholds in the bedrock river incision problem, *J. Geophys. Res.*, *108*(B2), 2117, doi:10.1029/2001JB001655.

Snyder, N. P., K. X. Whipple, G. E. Tucker, and D. J. Merritts (2003b), Correction to "Importance of a stochastic distribution of floods and erosion thresholds in the bedrock river incision problem", *J. Geophys. Res.*, *108*(B8), 2388, doi:10.1029/2003JB002649.

Stock, J., and D. R. Montgomery (1999), Geological constraints on bedrock river incision using the stream power law, *J. Geophys. Res.*, *104*, 4983–4993.

Tomkin, J., and J. Braun (1999), Simple models of drainage reorganization on a tectonically active ridge system, *N. Z. J. Geol. Geophys.*, *42*, 1–10.

Tomkin, J., M. T. Brandon, F. J. Pazzaglia, J. R. Barbour, and S. D. Willet (2003), Quantitative testing of bedrock incision models for the Clearwater River, NW Washington State, *J. Geophys. Res.*, *108*(B6), 2308, doi:10.1029/2001JB000862.

Tucker, G. E. (2004), Drainage basin sensitivity to tectonic and climatic forcing: Implications of a stochastic model for the role of entrainment and erosion thresholds, *Earth Surf. Processes Landforms*, *29*, 185–205, doi:10.1002/esp.1020.

Tucker, G. E., and R. L. Bras (2000), A stochastic approach to modeling the role of rainfall variability in drainage basin evolution, *Water Resour. Res.*, *36*(7), 1953–1964.

Tucker, G. E., and K. Whipple (2002), Topographic outcomes predicted by stream erosion models: Sensitivity analysis and intermodel comparison, *J. Geophys. Res.*, *107*(B9), 2179, doi:10.1029/2001JB000162.

van der Beek, P. A., and P. Bishop (2003), Cenozoic river profile development in the Upper Lachlan catchment (SE Australia) as a test of quantitative fluvial incision models, *J. Geophys. Res.*, *108*(B6), 2309, doi:10.1029/2002JB002125.

Vogt, H. (1992), *Le relief en Alsace, étude géomorphologique du rebord sud-occidental du Fossé Rhénan*, 239 pp., Ed. Oberlin, Strasbourg.

Whipple, K. X. (2001), Fluvial landscape response time: How plausible is steady-state denudation?, *Am. J. Sci.*, *301*, 313–325.

Whipple, K. X. (2004), Bedrock rivers and the geomorphology of active orogens, *Annu. Rev. Earth Planet. Sci.*, *32*, 151–185.

Whipple, K. X., and C. R. Trayler (1996), Tectonic control of fan size: The importance of spatially variable subsidence rates, *Basin Res.*, *8*, 351–366.

Whipple, K. X., and G. E. Tucker (1999), Dynamics of the stream-power incision model: Implication for heigth limits of mountain ranges, landscape response timescales, and research needs, *J. Geophys. Res.*, *104*, 17,661–17,674.

Whipple, K. X., and G. E. Tucker (2002), Implication of sediment-flux-dependent river incision models for landscape evolution, *J. Geophys. Res.*, *107*(B2), 2039, doi:10.1029/2000JB000044.

Whipple, K. X., G. S. Hancock, and R. S. Anderson (2000), River incision into bedrock: Mechanics and relative efficacy of plucking, abrasion and cavitation, *Geol. Soc. Am. Bull.*, *112*, 490–503.

Wobus, C., A. Heimsath, K. Whipple, and K. Hodges (2005), Active out-of-sequence thrust faulting in the central Nepalese Himalaya, *Nature*, *434*, 1008–1011, doi:10.1038/nature03499.

Zaprowski, B. J., E. B. Evenson, F. J. Pazzaglia, and J. B. Epstein (2001), Knickzone propagation in the Black Hills and northern High Plains: A different perspective on the late Cenozoic exhumation of the Laramide Rocky mountains, *Geology*, *29*, 547–550.

Zaprowski, B. J., F. J. Pazzaglia, and E. B. Evenson (2005), Climatic influences on profile concavity and river incision, *J. Geophys. Res.*, *110*, F03004, doi:10.1029/2004JF000138.

S. Carretier, Institut de Recherche pour le Développement, Laboratoire des Mécanismes de Transfert en Géologie, UMR 5563, 14 avenue Edouard Belin, F-31400 Toulouse, France. (carretie@lmtg.obs-mip.fr)

M. Giamboni, Bundesamt fr Umwelt - BAFUAbteilung Gefahrenprvention Schutzwald and Naturgefahren, CH-3003 Bern, Switzerland. (marzio.giamboni@buwal.admin.ch)

B. Nivière, Université de Pau et des pays de l'Adour, Avenue de l'Université, F-64000 Pau, France. (bertrand.niviere@univ-pau.fr)

T. Winter, Bureau de Recherches Géologiques et Minières, Aménagement et Risques Naturels, 14 av. C. Guillemin, F-45060 Orleans, France. (t.winter@brgm.fr)